Journal of Alloys and Compounds 986 (2024) 174112

Contents lists available at ScienceDirect

Journal of Alloys and Compounds

journal homepage: www.elsevier.com/locate/jalcom

Zero-thermal-quenching broadband yellow-emitting Bi^{3+}-activated phosphors based on metal to metal charge transfer

Ke Chen [a,b,1], Peixin Gao [a,b,1], Zengtao Zhang [a,b], Yibiao Ma [a,b], Zan Luo [a,b], Maxim S. Molokeev [c], Zhi Zhou [a,b,*], Mao Xia [a,b,*]

[a] School of Chemistry and Materials Science, Hunan Agricultural University, Changsha 410128, PR China
[b] Hunan Optical Agriculture Engineering Technology Research Center, Changsha, 410128, PR China
[c] World-Class Research Center "Advanced Digital Technologies", University of Tyumen, Tyumen 625003, Russia

ARTICLE INFO

Keywords:
Bi^{3+}-activated phosphors
Yellow-emitting
MMCT
Zero-thermal-quenching
WLED

ABSTRACT

Bi^{3+}-activated phosphors have been proven to have potential applications foreground in white light-emitting diodes (WLED), plant growth lamps and temperature sensing. Therefore, it is urgent to exploit high-efficiency Bi^{3+}-activated phosphors. Herein, a novel broadband yellow-emitting phosphor $Ba_2GdGaO_5:Bi^{3+}$ with high internal quantum efficiency (IQE = 77%) was obtained based on metal to metal charge transfer (MMCT) between Bi^{3+} ground state and Gd^{3+} excited states. The photoluminescence excitation (PLE) spectrum and photoluminescence (PL) spectrum range from 225 nm to 400 nm and 400 nm to 700 nm, respectively, which can avoid the reabsorption phenomenon efficiently. Besides, $Ba_2GdGaO_5:Bi^{3+}$ has superior thermal stability and it shows zero-thermal-quenching at 150 °C. The K^+ doping hardly changes the thermal stability and can improve the PL intensity to 133.1% when the K^+ concentration is 2%. Finally, a phosphor-convert WLED (pc-WLED) was simply synthesized by $Ba_2GdGaO_5:Bi^{3+}$ and $BaMgAl_{10}O_{17}:Eu^{2+}$ (BAM:Eu^{2+}) phosphors. The doping of Eu^{3+} can significantly enhance the color rendering index (CRI, from 88.1 to 91.5) and reduce the correlated color temperature (CCT, from 4911 K to 4014 K). The above experimental results demonstrated that the phosphor has great application prospect in WLED.

1. Introduction

In recent years, phosphor-converted LED (pc-LED) has developed rapidly and has wide range of applications in various fields [1,2]. The performance of pc-LED depends largely on the optical properties of phosphor, so it is necessary to develop high-performance phosphors [3–5]. At present, the most common phosphor is $Y_3Al_5O_{12}:Ce^{3+}$ (YAG:Ce^{3+}) yellow-emitting phosphor, which can emit white light by combing it with blue LED chip [6–8]. However, this type of WLED has a low CRI (< 75) and high CCT (> 5000 K), and doesn't fulfill the requirements for high-quality white lighting [9,10]. What's more, the strong blue light emitted by blue chip can affect human hormone secretion and harm human eyes [11,12]. A novel strategy using multi-emission phosphors and near-ultraviolet (n-UV) LED chip has been found to be effective in preventing blue light damage [13,14]. The key point of this strategy is to develop efficient n-UV excited phosphors.

Rare earth luminescent materials have been commercialized, such as Eu^{2+}-activated phosphors and Ce^{3+}-activated phosphors [15–17]. The PLE spectra of these phosphors usually includes blue and even green regions, and the PLE spectra and PL spectra overlap. These characteristics may lead to reabsorption phenomenon, reduce the luminescence efficiency of pc-LED, resulting in white-light distortion [18,19]. Transition metal Mn^{4+}-activated fluoride phosphor exhibited bright narrow red emitting, but the excitation spectrum is range from 200 to 600 nm, which also caused reabsorption [20,21]. Furthermore, the preparation process of fluoride phosphor needs to use hydrofluoric acid, which may cause harm to the human body, and lead to environmental pollution [22]. These shortcomings greatly limit the application of this kind of phosphor.

Trivalent bismuth (Bi^{3+}), has drawn wide attention owing to the characteristic absorption in the UV region (6 s → 6p transition). Bi^{3+} has nearly no absorption in visible region, which can prevent the reabsorption phenomenon [23–25]. Another notable advantage of Bi^{3+} ion is its spectral tunability performance [26–28]. However, this can also lead

* Corresponding authors at: School of Chemistry and Materials Science, Hunan Agricultural University, Changsha 410128, PR China.
E-mail addresses: zhouzhi@hunau.edu.cn (Z. Zhou), xiamao2019@hunau.edu.cn (M. Xia).
[1] Ke Chen and Peixin Gao contributed equally to this work.

https://doi.org/10.1016/j.jallcom.2024.174112
Received 4 December 2023; Received in revised form 7 March 2024; Accepted 7 March 2024
Available online 8 March 2024

to unpredictable behavior and uncontrollable situations. Both opportunities and challenges exist, and this double-edged sword opens up the possibility of spectrally efficient modulation of Bi^{3+}. The electronic configuration of the element Bi is [Xe]$4f^{14}5d^{10}6\ s^26p^3$, in which the 6 s orbital loses one electron and the 6p orbital loses two electrons, so the electronic configuration of Bi^{3+} is [Xe]$4f^{14}5d^{10}6$ s6p, and its outermost electron orbital is 6s and 6p. Therefore, because of the naked 6s and 6p outer electrons, Bi^{3+} is sensitive to the surrounding crystal field environment, resulting in multicolor emission [23,29–31]. However, most of Bi^{3+}-activated phosphors represent blue, cyan or green emission, such as $Sc_2Si_2O_7$:Bi^{3+} (deep-blue emitting),[32] $CaGdGaO_6$:Bi^{3+} (blue emitting),[33] Sr_2GdGaO_5:Bi^{3+} (cyan emitting),[34] and Ba_2LaGaO_5:Bi^{3+} (green emitting) [35]. Compared with these emission bands, yellow lights have more contribution to improve CRI and reduce CCT of pc-WLED. At present, there is a lack of Bi^{3+} activated phosphors that emit yellow/orange light, and some of the only yellow/orange light still has many drawbacks. Lin reported a series of $ABZn_2Ga_2O_7$:Bi^{3+} (A = Ca, Sr; B = Ba, Sr) phosphors with yellow/orange-emitting and achieved excellent CRI of 97.9. Unfortunately, neither IQE (< 25%) nor thermal stability (< 50% at 423 K) is satisfactory, which needs to be further improved [36]. Other yellow/orange phosphors such as Ba_2ZnWO_6:Bi^{3+}, K_2MgGeO_4:Bi^{3+} and $SrLaZnO_{3.5}$:Bi^{3+} also have similar defects [37–39]. Consequently, it is of great importance to explore efficient yellow/orange-emitting Bi^{3+}-activated phosphors, not only to fill the gap of Bi^{3+}-activated phosphors, but also to achieve more efficient white light lighting.

Recently, a novel strategy for constructing electron energy levels interact between Bi^{3+} and cations with d^0 or d^{10} configuration was proposed, and the corresponding state is called MMCT state [40]. Bi^{3+}-activated phosphor with the luminescence behavior from MMCT state to Bi^{3+} ground state has large stokes shift, which can be used to guide the realization of yellow/orange emission. In this work, a broad yellow-emitting Ba_2GdGaO_5:Bi^{3+} phosphor was synthesized based on MMCT between Bi^{3+} ground state and Gd^{3+} excited states. This phosphor has excellent comprehensive properties, with IQE up to 77% and zero thermal quenching at 150 °C. In addition, K^+ ions were added as fluxing agent to further improve the emission intensity. When K^+ concentration was 2 mol%, the emission intensity increased to 133% of the original. Finally, a yellow LED was prepared by Ba_2GdGaO_5:Bi^{3+} phosphor and 365 nm n-UV chip, which have a high color purity of 82.4%. A pc-WLED with a high CRI of 88.1 and a low CCT of 4911 K was fabricated by Ba_2GdGaO_5:Bi^{3+} and BAM: Eu^{2+} phosphors. Eu^{3+} ion was introduced into the prepared yellow phosphor to further improve the CRI (91.5) and reduce the CCT (4014 K) of the pc-WLED. All the results demonstrated that Ba_2GdGaO_5:Bi^{3+} phosphor as a candidate material for achieving high quality WLED.

2. Experiment section

2.1. Materials and synthesis

The raw materials of these phosphor are $BaCO_3$ (99.99%, Aladdin), Gd_2O_3 (99.99%, Aladdin), Ga_2O_3 (99.99%, Aladdin), Bi_2O_3 (99.99%, Aladdin), K_2CO_3 (99.99%, Aladdin), and Eu_2O_3 (99.99%, Aladdin). All of these phosphors Ba_2GdGaO_5:x mol%Bi^{3+} (x = 0, 0.5, 1, 2, 3, 4, 5), Ba_2GdGaO_5:3 mol%Bi^{3+}, y mol%K^+ (y = 0, 0.5, 1, 1.5, 2), Ba_2GdGaO_5:3 mol%Bi^{3+}, n mol%Eu^{3+} (n = 0, 0.5, 1, 2, 3, 4, 5) were prepared by high-temperature solid-state method. The experiment steps are as follows: i) An analytical balance was used to weigh these ingredients by stoichiometric ratio, and then placed them in an agate mortar. ii) 2–3 mL anhydrous ethanol was added in agate mortar and ground them adequately for 40 minutes. iii) The mixture was poured into a corundum crucible and placed in the muffle furnace, the sintering condition was 1300 °C/6 h. iv) After the furnace cooled to its natural temperature, the specimens were taken and ground to a fine powder for subsequent testing. The pc-LEDs were fabricated by Ba_2GdGaO_5:Bi^{3+}, BAM:Eu^{2+} phosphors and 365 nm n-UV chips. The steps are as follows: i) The epoxy resin A and B were combined in a ratio of 1:2. ii) The phosphors and epoxy resin are thoroughly mixed until thick. iii) The mixture was coated on LED chips and placed in an oven at 90 °C for 18 hours. After drying, pc-LEDs were obtained.

2.2. Characterization

X-ray diffraction (XRD) data were recorded using an Aries X-ray diffractometer (PANalytical, Netherlands) fitted with monochromatic Cu Kα radiation (40 kV, 15 mA). The increment between steps of 2θ was 0.022°, and the duration of each counting period was 18.87 s. Rietveld refinement was accomplished by using TOPAS 4.2. PL and PLE spectra were measured on an F-4700 fluorescence spectrometer (Hitachi, Japan). Temperature-dependent PL spectra were recorded by an F-4700 fluorescence spectrometer with a heat controller (Orient KOJI, China). X-ray photoelectron spectroscopy (XPS) spectrum was measured on an X-ray photoelectron spectrometer (Thermo escalab 250Xi, U.S.). IQE and decay time were collected using a FLS-1000 fluorescence spectrometer (Edinburgh, U.K.). Diffuse reflection (DR) and electroluminescence (EL) spectra were obtained by ultraviolet and visible spectrophotometer (Shimadzu, Japan) and photoelectric test system (Everfine, China), respectively.

3. Results and discussion

3.1. Crystal structure and phase purity

Fig. 1 is the crystal structure diagram and Rietveld refinement pattern of Ba_2GdGaO_5 host material. The refinement results (Table 1 and Table 2) indicate that all diffraction peaks can be indexed by monoclinic cell ($P2_1$) with parameters close to Ba_2NdAlO_5. Therefore, this structure was used as the starting model for the Rietveld. The refinement was performed using TOPAS 4.2. When the sites of Nd^{3+} and Al^{3+} ions were occupied by Gd^{3+} and Ga^{3+} ions, respectively. the target material Ba_2GdGaO_5 was obtained. Refinements remained stable and gave low R-factors (R_{wp} = 6.13, R_p = 4.66, R_B = 0.9 and χ^2 = 1.36). Crystal structure Ba_2GdGaO_5 consists of GdO_6 distorted octahedra which joints with GaO_4 tetrahedra forming 3D net, and Ba^{2+} ion locates in holes of this 3D net. Bi^{3+} tends to substitute six-coordination sites instead of four-coordination sites. Additionally, the ionic radius of Bi^{3+} (CN = 6, r =

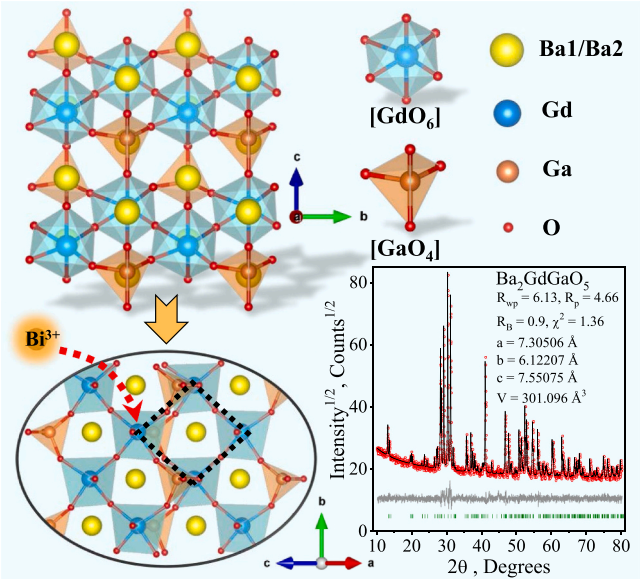

Fig. 1. Crystal structure in different crystal axis directions and XRD Rietveld refinements of Ba_2GdGaO_5 host material.

Table 1
Main parameters of processing and refinement of the Ba_2GdGaO_5.

sample	Space Group	Cell parameters (Å), Cell Volume (Å^3)	R_{wp}, R_p, R_B, χ^2
Ba_2GdGaO_5	$P2_1$	a = 7.30506(15), b = 6.12207(12), c = 7.55075(15), V = 301.096(11)	6.13, 4.66, 0.9, 1.36

Table 2
Main bond lengths (Å) of Ba_2GdGaO_5.

Ba_2GdGaO_5			
Ba1—O1	2.679(36)	Ba1—O2^{i}	3.0746(44)
Ba1—O2^{ii}	3.133(39)	Ba1—O3^{i}	3.202(65)
Ba1—O3^{iii}	2.625(68)	Ba1—O4^{iv}	3.430(46)
Ba1—O4^{iii}	2.706(60)	Ba1—O5^{v}	2.758(48)
Ba1—O5^{iii}	3.284(60)	Ba2—O1	3.0977(42)
Ba2—O2	2.689(38)	Ba2—O3	2.89(10)
Ba2—O3^{iii}	2.92(10)	Ba2—O4	2.700(43)
Ba2—O4^{vi}	3.439(58)	Ba2—O5	3.449(43)
Ba2—O5^{vii}	2.707(59)	Gd—O1	2.416(36)
Gd—O2^{iii}	2.301(44)	Gd—O3^{i}	2.151(93)
Gd—O3^{iii}	2.264(81)	Gd—O4^{i}	2.231(56)
Gd—O5	2.329(49)	Ga—O1^{vii}	1.827(47)
Ga—O2^{viii}	1.891(41)	Ga—O4	1.871(50)
Ga—O5	1.897(58)		

1.03 Å) is similar to that of Gd^{3+} (CN = 6, r = 0.938 Å). Therefore, Bi^{3+} is supposed to occupy GdO_6 site to form a luminescent center, resulting in a yellow phosphor Ba_2GdGaO_5:Bi^{3+}.

Fig. 2a shows XRD patterns of phosphors doped with different concentrations of Bi^{3+}. All diffraction peaks match well with the calculated result, demonstrating that doping the material with Bi^{3+} from 0 mol% to 5 mol% doesn't affect its structure. Fig. 2b is the XRD patterns of Ba_2GdGaO_5:3 mol%Bi^{3+}, y mol%K^+ (y = 0, 0.5, 1, 1.5, 2) phosphors and all these samples are pure phase. Fig. 2c is the XRD patterns of Eu^{3+} ions co-doped with different concentrations. The Bi^{3+} ion concentration stays at 3 mol%, and the Eu^{3+} ion concentration ranges from 0 mol% to 5 mol %. A series of Ba_2GdGaO_5:3 mol%Bi^{3+}, n mol%Eu^{3+} (n = 0–5) phosphors are obtained. Their XRD has basically no change, proving that all the samples are well synthesized.

3.2. Luminescence performance

Fig. 3a illustrates the PLE spectra of Ba_2GdGaO_5:x mol%Bi^{3+} phosphors. The excitation band is predominantly located in the near ultraviolet range between 300 and 400 nm. The excitation peak is 342 nm and is attributed to the $^1S_0 \rightarrow {}^3P_1$ transition of Bi^{3+}. The excitation is in good agreement with the emission band of commercial n-UV chip. In addition, there is a weak excitation band range from 225 nm to 275 nm, which ascribe to $^1S_0 \rightarrow {}^1P_1$ transition. As shown in Fig. 3b, the emission spectra of Ba_2GdGaO_5:x mol%Bi^{3+} phosphors show broadband emission from 380 nm to 700 nm with peak at 547 nm. As the concentration of Bi^{3+} increases, the PL intensity of the phosphor initially increased, but subsequently decreased. The maximum intensity was achieved at x = 3 mol%. The reduction of PL intensity is caused by the concentration quenching produced by the high concentration of Bi^{3+} ion. To enhance comprehension of concentration quenching's mechanism, we calculated the critical distance via the subsequent equation: [41,42]

$$R_c \approx 2 \times \left(\frac{3V}{4\pi x_c n}\right)^{\frac{1}{3}} \quad (1)$$

where the V is cell volume,x_c is critical doping concentration, n represent the available site occupied by the activator ion. In this material, V, x_c and n are 301.096 Å, 0.03 and 2, respectively. The critical distance was calculated to be 21.241 Å, which beyond the exchange interaction distance (5 Å). Hence, multiple interaction is considered to have a significant impact on concentration quenching between Bi^{3+} ions. According to Dexter's theory, when the concentration burst is a multiple interaction, the strength of this interaction can be determined by the intensity of its luminescence spectrum. To obtain Fig. 6(a), we fit lg(I/x) and lg(x) using the following equation:[5,43]

$$\frac{I}{x} = k[1 + \beta(x)^{\frac{\theta}{a}}]^{-1} \quad (2)$$

where k and β represent certain excitation conditions and specific matrix crystals, x represents the doping concentration of Bi^{3+}, and I represents the luminescence intensity of the phosphor of the corresponding concentration of x. The slope of the fitted line in Fig. 3c was obtained by calculation to be −1.1765, and so the value of θ was calculated to be 3.5295, which is closer to 6. Therefore, it can be proved that the concentration burst mechanism in Ba_2GdGaO_5: Bi^{3+} phosphor is caused by dipole-dipole interactions.[44] Fig. 3d is the relationship between emission intensity and Bi^{3+} doping concentration. Moreover, the peak value of the PL spectra is slightly shifted when the concentration of Bi^{3+} increases. As mentioned above, the luminescence behavior of Bi^{3+} ion is closely related to the change of crystal field environment. Different concentrations of Bi^{3+} ions doped will affect the crystal field environment around the luminescence center, leading to slight changes in the

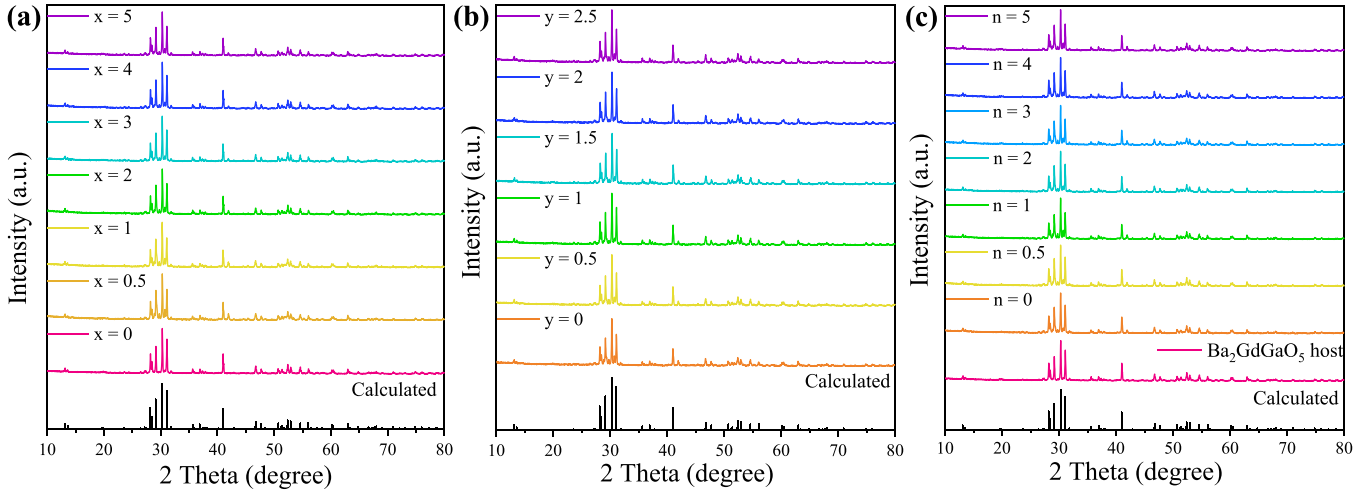

Fig. 2. XRD patterns of (a) the Ba_2GdGaO_5:x mol%Bi^{3+}, (b) the Ba_2GdGaO_5:3 mol%Bi^{3+}, y mol%K^+ and (c) the Ba_2GdGaO_5:3 mol%Bi^{3+}, n mol%Eu^{3+} phosphors.

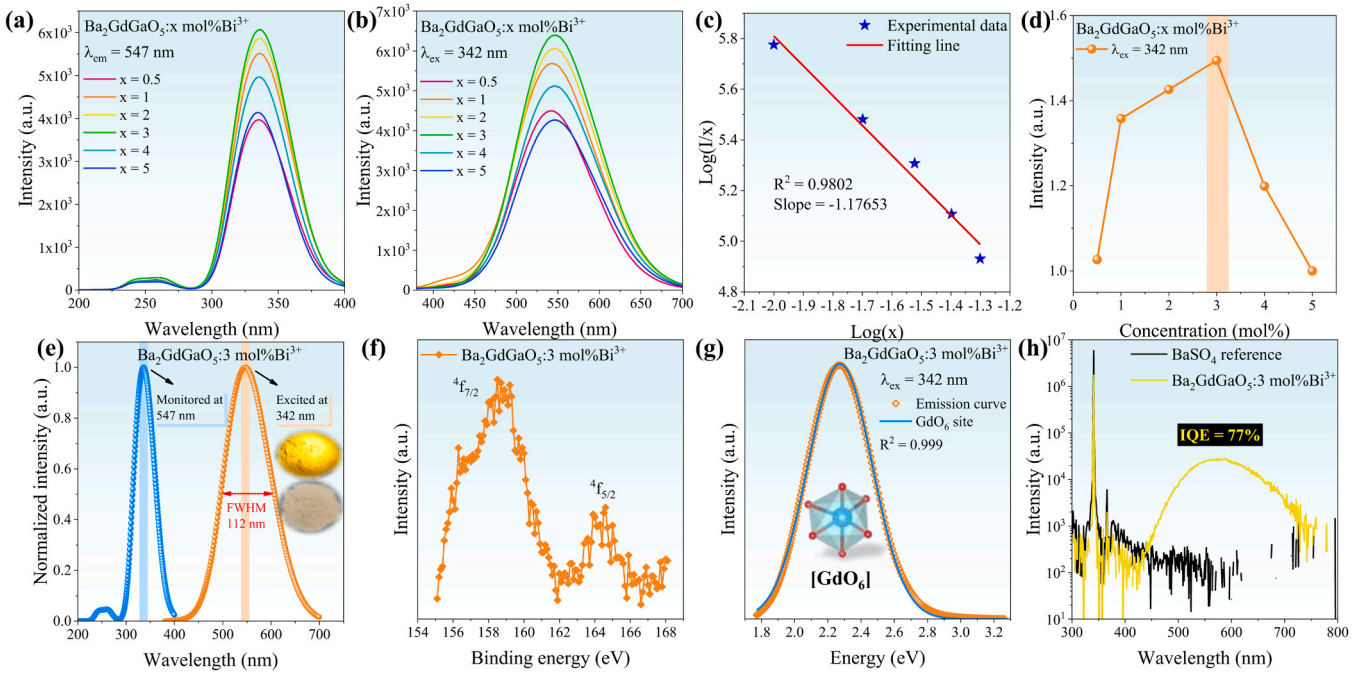

Fig. 3. (a) PLE and (b) PL spectra of Ba_2GdGaO_5:x mol%Bi^{3+} phosphors. (c)The relationship between Log(I/x) and Log(x). (d) The relationship between emission intensity and Bi^{3+} doping concentration. (e) PLE and PL spectra of Ba_2GdGaO_5:3 mol%Bi^{3+} and its photographs. (f) The XPS spectrum. (g) Gaussian fitting of the PL spectrum of Ba_2GdGaO_5:3 mol%Bi^{3+} under excitation of 342 nm. (h) The IQE of Ba_2GdGaO_5:3 mol%Bi^{3+}.

crystal field splitting strength, resulting in peak displacement phenomenon. Fig. 3e illustrates the optimal PL and PLE spectra of Ba_2GdGaO_5:3 mol%Bi^{3+} phosphor. The full width at half-maximum (FWHM) of PLE spectrum reaches 112 nm and has a large Stokes shift. Hence, the PLE spectrum and PL spectrum hardly overlap, which can effectively avoid reabsorption. The illustrations are pictures of Ba_2GdGaO_5:3 mol% Bi^{3+} phosphor under natural light and 365 nm n-UV light. It can be seen that the phosphor is milky white under natural light, while it shows strong yellow light emission under n-UV light.

The XPS spectrum (Fig. 3f) shows that the Ba_2GdGaO_5:3 mol%Bi^{3+} phosphor has a characteristic peak near 159 eV and 164 eV, which is attributed to Bi^{3+} $^4f_{7/2}$ and Bi^{3+} $^4f_{5/2}$. This result proves that the valence state of bismuth element is trivalent. To further confirm the occupation of Bi^{3+} and the number of luminescent centers, a Gaussian fitting is carried out for the PL spectrum of Ba_2GdGaO_5:3 mol%Bi^{3+} phosphor. As shown in Fig. 3g, the spectral curve can be well fitted by a single peak and the value of R^2 is as high as 0.999, which indicates that the fitting result is reliable. Therefore, it can be confirmed that Bi^{3+} ion will only replace GdO_6 site to form one luminescent center. The quantum efficiency is a key index to evaluate the luminescence performance of phosphor. In Fig. 3h, in contrast to the white board coated with $BaSO_4$, the IQE of Ba_2GdGaO_5:3 mol%Bi^{3+} phosphor reaches 77% under the excitation of 342 nm n-UV light. This test results show that it has excellent luminescent properties. Relevant equation as follows:[45]

$$\eta_{IQE} = \frac{\int L_s}{\int E_R - \int E_s} \tag{3}$$

where η_{IQE} and L_S are the value of IQE and PL spectrum, respectively. E_R and E_S represent the spectrum of the excitation light with and without sample in integrating sphere.

In the preparation of phosphors, adding a small amount of flux materials is beneficial to reduce the sintering temperature. In addition, the flux materials can also cause the carbonate or nitrate in the raw material to decompose more thoroughly and improve the crystallinity of the resulting phosphor particles. Thus, it is beneficial to enhance the luminescent performance of phosphor. Alkali metal ions are common flux materials and have been successfully utilised in various phosphor systems to enhance their luminescence performance, such as $CaYGaO_4$:Bi^{3+} and $BaScO_2F$:Bi^{3+} phosphors. As shown in Fig. 4a-d, we co-doped K^+ ion as flux materials to improve the PL intensity of Ba_2GdGaO_5:3 mol%Bi^{3+} phosphor. Fig. 4b-c display the PL spectra of Ba_2GdGaO_5:3 mol%Bi^{3+}, y mol%K^+ phosphors excited at 342 nm and 365 nm, respectively. The PL intensity all increase with K^+ concentration doping. We plotted the relationship between emission intensity and K^+ ion concentration in Fig. 4d. When the concentration of K^+ reaches 1.5 mol%, the intensity increases to 121.1% of the initial intensity excited at 342 nm. Moreover, under the excitation of 365 nm, the PL intensity can enhance to 133.1% when y = 2 mol%. As mentioned above, the K^+ doping has no effect on the phase (in Fig. 2b). Therefore, the function of K^+ ions is to act as a flux to improve the crystallinity of Ba_2GdGaO_5:3 mol%Bi^{3+} phosphor and thus improve the luminescent intensity. Fig. 4e presents the decay lifetime curves of Ba_2GdGaO_5:3 mol%Bi^{3+} and Ba_2GdGaO_5:3 mol%Bi^{3+}, 2 mol%K^+ phosphors monitored at 547 nm at room temperature. Both of these phosphors possess only one luminescent center, hence their decay curves fit perfectly with a single exponential function, as shown below:[46–48]

$$I(t) = I_0 \times A\exp\left(-\frac{t}{\tau}\right) \tag{4}$$

where $I(t)$ and I_0 are the PL intensity at time t and time 0, respectively. A and τ are constant and decay time of fluorescence lifetime, respectively. The lifetime values of Ba_2GdGaO_5:3 mol%Bi^{3+} and Ba_2GdGaO_5:3 mol% Bi^{3+}, 2 mol%K^+ phosphors are calculated to be 351.21 ns and 347.48 ns. It can be seen from Fig. 4e that the lifetime value of doped K^+ hardly changes. Fig. 4f gives the DR spectra of Ba_2GdGaO_5, Ba_2GdGaO_5:3 mol%Bi^{3+} and Ba_2GdGaO_5:3 mol%Bi^{3+}, 2 mol%K^+ phosphors. The obvious absorption band around 250 nm in the host material is attributed to the electron transition between the valence and conduction bands. After doping Bi^{3+} ion, the absorption of these phosphors in the n-UV region (250–400 nm) is significantly stronger, and the absorption wavelength matches well with the excitation spectrum. The optical bandgap of Ba_2GdGaO_5 can be calculated through:[49–51]

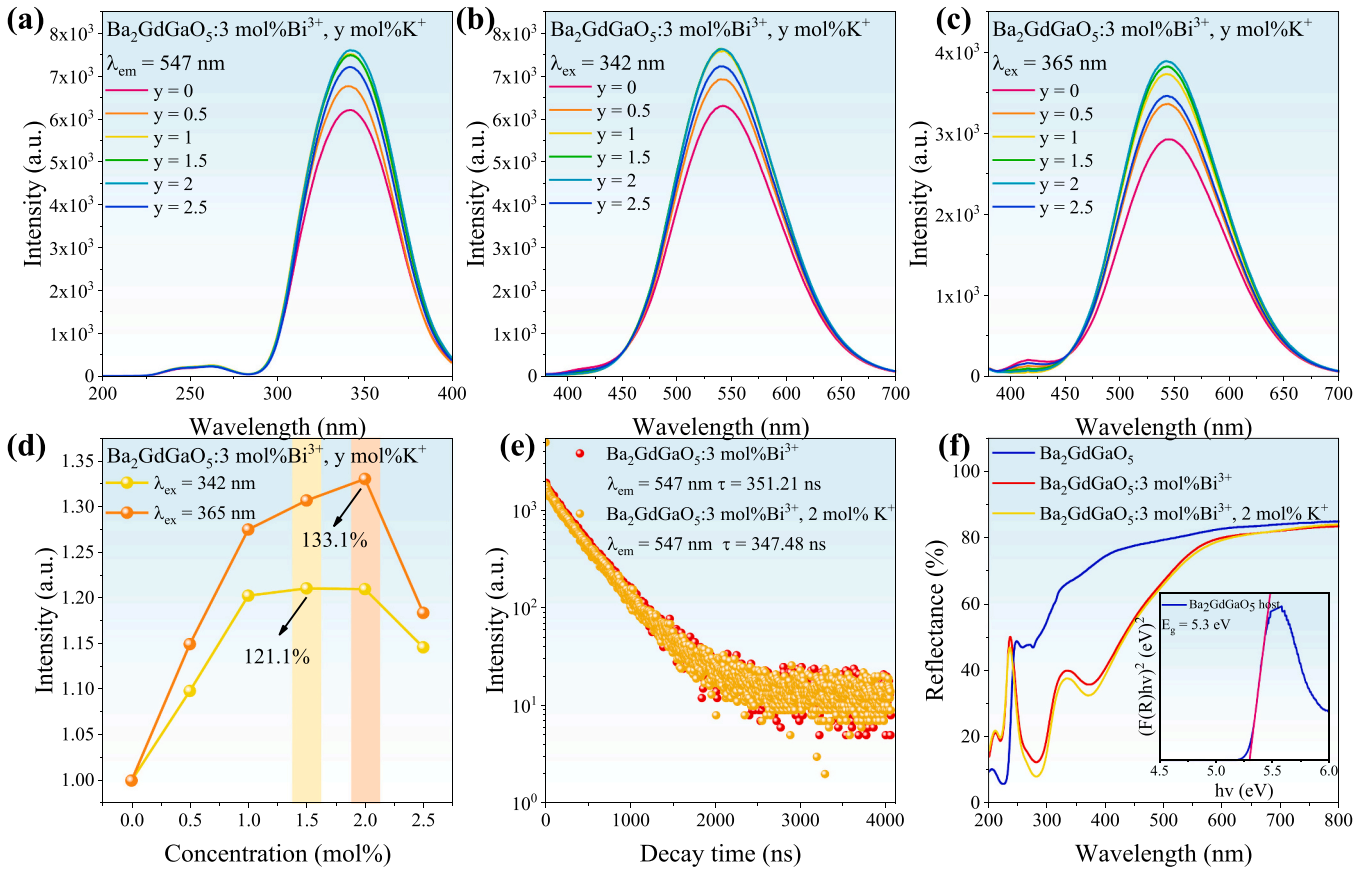

Fig. 4. (a) PLE and (b-c) PL spectra of Ba_2GdGaO_5:3 mol%Bi^{3+}, y mol%K^+ phosphors. (d) The relationship between emission intensity and K^+ doping concentration. (e) The decay curves of Ba_2GdGaO_5:3 mol%Bi^{3+} and Ba_2GdGaO_5:3 mol%Bi^{3+}, 2 mol%K^+ phosphors. (f) DR spectra of Ba_2GdGaO_5, Ba_2GdGaO_5:3 mol%Bi^{3+} and Ba_2GdGaO_5:3 mol%Bi^{3+}, 2 mol%K^+, insert figure is the calculation of optical band gap.

$$F(R) = (1-R)^2/2R \tag{5}$$

$$\left(F(R)hv\right)^{\frac{1}{n}} = A\left(hv - E_g\right) \tag{6}$$

where $F(R)$, R, hv and E_g represent absorption, reflection (%), photon energy and optical band gap, respectively. It is known that similar Ba_2YGaO_5 material is a direct bandgap,[52] so the n value is 1/2, and the band gap value is calculated to be 5.3 eV (illustration in Fig. 4f).

In main lattice Ba_2GdGaO_5, the interaction of Bi^{3+} dopants with the nearest neighbouring Ga^{3+} and Gd^{3+} ions results in the appearance of two d-energy level states in the bandgap corresponding to Bi^{3+}-Ga^{3+} MMCT and Bi^{3+}-Gd^{3+} MMCT, respectively. These abundant electron leaps result in significant photoluminescent properties of Bi^{3+}-activated Ba_2GdGaO_5. At the same time, we calculated the values of the d-energy states (Bi^{3+}-Ga^{3+} MMCT and Bi^{3+}-Gd^{3+} MMCT) using the empirical equations proposed by Philippe Boutinaud:[23,40]

$$MMCT\left(Bi^{3+}, cm^1\right) = \frac{\chi_{CN=4}(Ga^{3+})}{d_{corr}} \tag{7}$$

which is valid for 4-coordinated Ga^{3+} metals, and

$$MMCT(Bi^{3+}, cm^1) = \frac{\chi_{CN>4}(Gd^{3+})}{d_{corr}} \tag{8}$$

which is valid for 6-coordinated Gd^{3+} metals, and

$$d_{corr} = d_{host} + \frac{1}{2}[r(Bi^{3+}) - r(host)] \tag{9}$$

In these equations, $\chi_{CN=4}(Ga^{3+})$ and $\chi_{CN=6}$ (Gd^{3+}) represent the optical electronegativity of Ga^{3+} and Gd^{3+}, respectively. The variable d_{host} represents the shortest key length of Bi^{3+}-Gd^{3+}. The variables r (Bi^{3+}) and r(host) represent the ionic radius of Bi^{3+} and the ionic radius of Bi^{3+} occupying the matrix cation Gd^{3+}, respectively.[40] Based on the above equations and data in Table 3, the Bi^{3+}-Ga^{3+} MMCT value is approximately 47714 cm^{-1} (210 nm) in the ultraviolet. This value should be disregarded. The Bi^{3+}-Gd^{3+} MMCT value is approximately 40748 cm^{-1} (245 nm), which corresponds to the weak peak in the excitation spectrum (250 nm). Hence, it can be concluded that Bi^{3+}-Gd^{3+} MMCT contributes to luminescence. Luminescence mechanism diagram of Ba_2GdGaO_5:Bi^{3+} phosphor is shown in Fig. 5. Under the excitation of n-UV light, the electrons transition from the ground state of $^1S_0$ to the excited state of $^3P_1$. After which the nonradiative relaxation occurs to the lowest position of the MMCT state and a large Stokes shift creates. Finally, the electrons return to their ground state by a radiative transition, accompanied by intense yellow light emission. The MMCT state comes from the interaction between Bi^{3+} levels and the Gd^{3+} (d^0 configuration) excited states.

3.3. Spectral tunability and zero-thermal-quenching performance

To achieve the spectral tunability performance, we continue to doping another activator Eu^{3+} to get Ba_2GdGaO_5:3 mol%Bi^{3+}, n mol%

Table 3
Theoretical energy values of the MMCT states of Ba_2GdGaO_5:Bi^{3+} from the semi-empirical model.

sample	χ_{CN} (M^{n+})	d_{corr} (Å)	MMCT (cm^{-1})
Ba_2GdGaO_5:Bi^{3+}	1.386(Gd^{3+}) 1.755(Ga^{3+})	4.425(Bi^{3+}-Gd^{3+}) 4.095(Bi^{3+}-Ga^{3+})	40748 47714

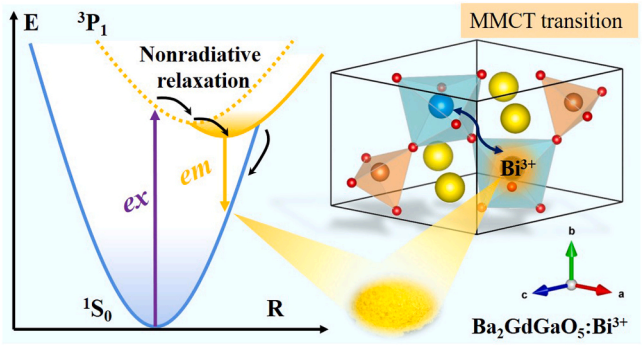

Fig. 5. Luminescence mechanism diagram of $Ba_2GdGaO_5:Bi^{3+}$ phosphor.

Eu^{3+} (n = 0–5) phosphors. It has been previously analyzed that doping of Eu^{3+} will not affect their phase (in Fig. 2c). The PL spectra are exhibited in Fig. 6a, as the concentration of Eu^{3+} increases, the emission of several typical Eu^{3+} ions at 600 nm narrow band red light gradually enhanced. When n = 4 mol%, the red light reaches maximum. However, when the concentration increased further, the red light began to weaken, which may be due to the competition between Bi^{3+} and Eu^{3+} ions. According to CIE chromaticity coordinates (Fig. 6b), with increasing Eu^{3+} ion concentration, the chrominance coordinates are gradually moving towards the red zone. The corresponding phosphor photographs are shown in Fig. 6c. Under 365 nm n-UV light, the color of these phosphors gradually changes from yellow light to orange red light. These phosphors still appear milky white under natural light, and no significant changes have occurred.

The thermal quenching resistance of phosphors is also an important index to evaluate their luminescent properties. The temperature-dependent emission spectra of Ba_2GdGaO_5:3 mol%Bi^{3+} and Ba_2GdGaO_5:3 mol%Bi^{3+}, 2 mol%K^+ phosphors are presented in Fig. 7. The PL spectra in the range of 25 °C to 300 °C at 342 nm excitation were measured. With the increase of temperature, the PL intensity of these two phosphors both initially increase and then decrease. The normalized temperature-dependent PL spectra (Fig. 7b, e) show a blue shift in the peak wavelength of both phosphors from 547 nm blue to 527 nm and from 551 nm blue to 531 nm, respectively. The reason for this phenomenon may be the increase in population of higher vibrational levels of the local Bi^{3+} radiation center with increasing temperature. Moreover, as the temperature increases, the lattice will expand and the crystal field will weaken, resulting in blue shift of spectra. In the next stage, we calculated the integral area of the emission spectra and expressed it as the Integrated PL intensity, as shown in Fig. 7 f. When the temperature reaches 150 °C, the Integrated PL intensity of Ba_2GdGaO_5:3 mol%Bi^{3+} and Ba_2GdGaO_5:3 mol%Bi^{3+}, 2 mol%K^+ maintained 101% and 98.2% of the initial intensity respectively, achieving zero thermal quenching. When the temperature reaches 250 °C, the luminescent thermal quenching can still be about 20%. In the actual production application, the luminous intensity of phosphor at 85 ℃ and 105 ℃ is an important index to evaluate the lamp bead. We conducted relevant tests, as shown in Fig. 7 f. It can be found that the luminescent intensity of the phosphor Ba_2GdGaO_5:3 mol%Bi^{3+} at 85 ℃ and 105 ℃ is 107% and 108% of that at room temperature (25 ℃), respectively. Meanwhile, the luminescent intensity of phosphor Ba_2GdGaO_5:3 mol%Bi^{3+}, 2 mol%K^+ at both 85 °C and 105 °C were 100% of that at room temperature. The slight change of thermal stability is related to the modification of grain after adding the flux. Therefore, these phosphors have strong thermal quenching resistance. This abnormal heat quenching may be attributed to the defects of the host material, which can capture photons and generate thermal stimulation radiation benefits. The defect energy level dominates when the temperature is high and it can compensate the light loss caused by thermal quenching. Therefore, the luminescent intensity will increase first. When the temperature is too high, thermal quenching is dominant, so the luminescence intensity decreases.

3.4. WLED application

To verify the application possibility of Ba_2GdGaO_5:3 mol%Bi^{3+} phosphor, a series of pc-LED were prepared with 365 nm n-UV chips. In Fig. 8a, the first is the EL spectrum of pc-LED prepared with Ba_2GdGaO_5:3 mol%Bi^{3+} phosphor. It exhibits a broadband yellow light emitting with a color purity of 82.4% and corresponding CIE coordinates of (0.4527, 0.4877). A pc-WLED (LED2) was obtained by combining this phosphor with commercial BAM:Eu^{2+}. The CIE coordinate was (0.3472, 0.3490), CCT was 4911 K, and CRI reached 88.1. By introducing Eu^{3+} ions and increasing the red part of the spectrum, a LED3 with higher CIR of 91.5 was obtained. The CIE coordinate of the LED3 was shifted to the red light region (0.3737, 0.3530), and the CCT further decreased to 4014 K, which was typical warm white light emitting.

4. Conclusion

In conclusion, a novel zero-thermal-quenching broadband yellow-emitting Bi^{3+}-activated $Ba_2GdGaO_5:Bi^{3+}$ phosphor was synthesized based on MMCT transition. The FWHM is 112 nm and the IQE reaches 77%. When the temperature is heated up to 150 °C, the PL intensity can be maintained at 101% of normal temperature. The corresponding

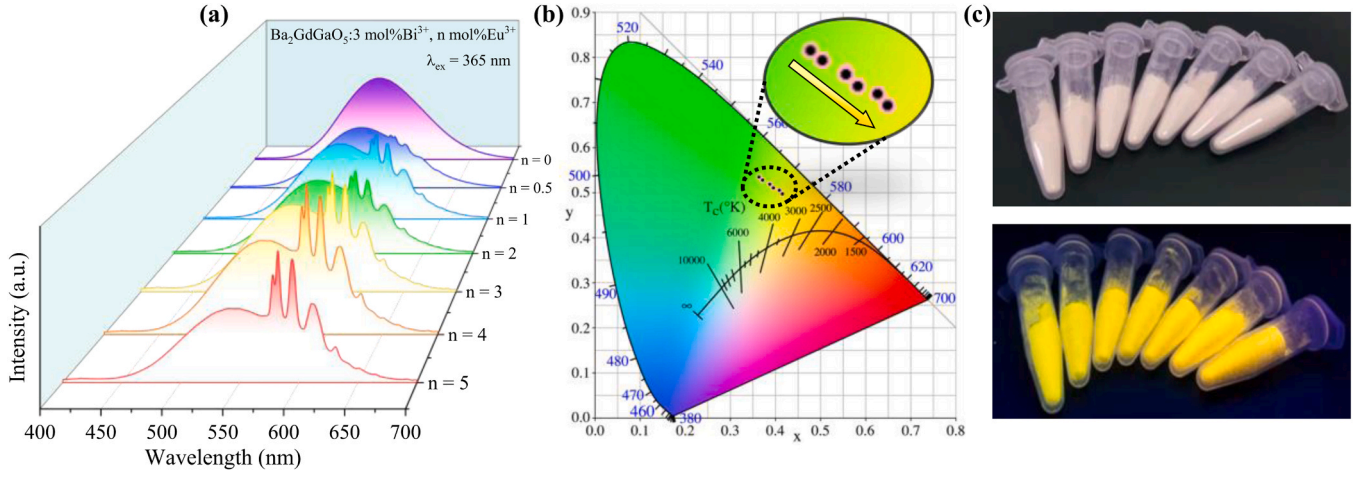

Fig. 6. (a) The PL spectra and (b) CIE chromaticity of Ba_2GdGaO_5:3 mol%Bi^{3+}, n mol%Eu^{3+} (n = 0–5) phosphors. (c) The photographs under natural light and 365 nm n-UV light.

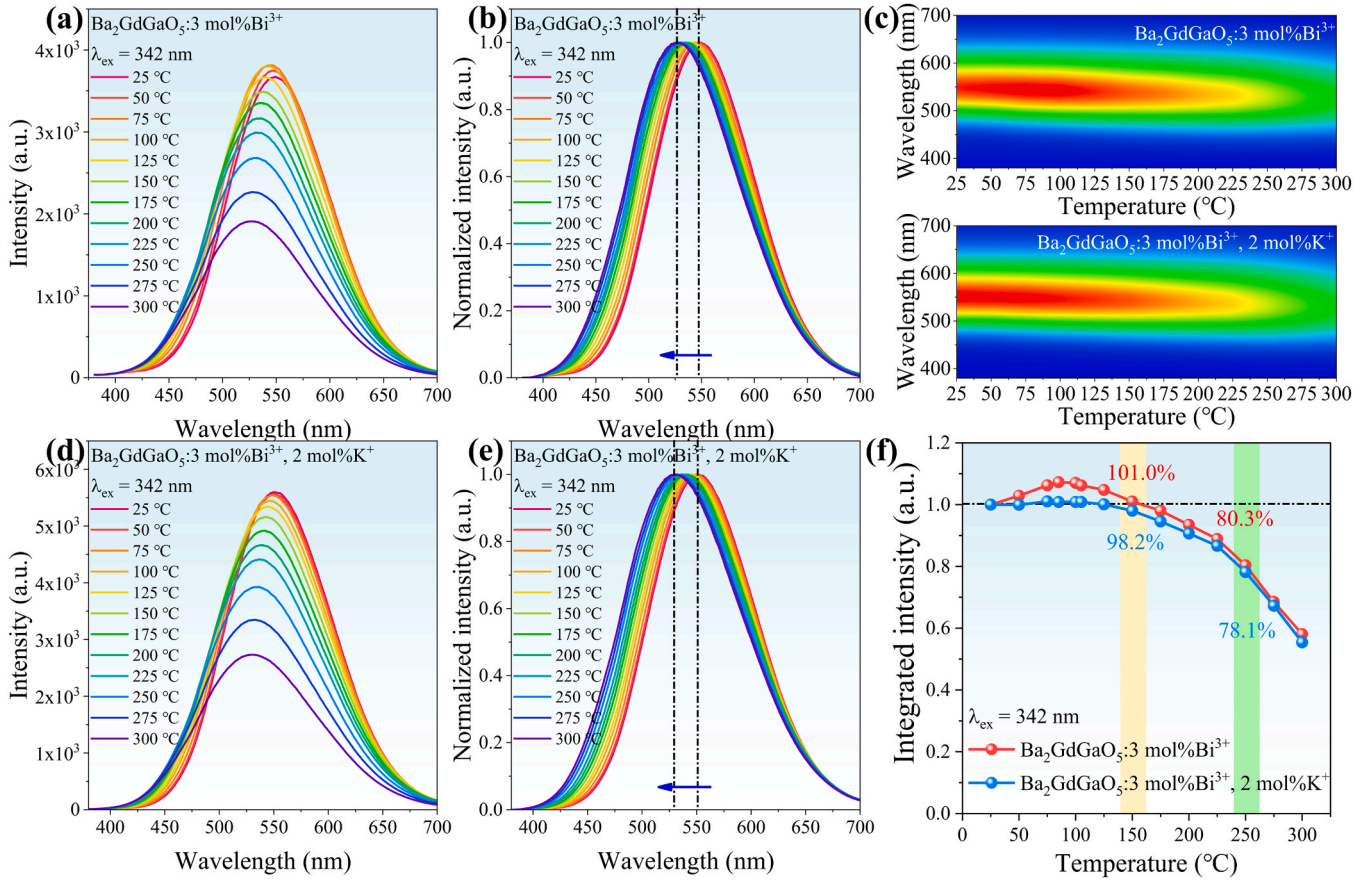

Fig. 7. (a-b) Temperature-dependent and normalized temperature-dependent PL spectra from 25°C to 300 °C of Ba_2GdGaO_5:3 mol%Bi^{3+}. (c) Temperature-dependent PL spectra of Ba_2GdGaO_5:3 mol%Bi^{3+} and Ba_2GdGaO_5:3 mol%Bi^{3+}, 2 mol%K^+. (d-e) Temperature-dependent and normalized temperature-dependent PL spectra of Ba_2GdGaO_5:3 mol%Bi^{3+}, 2 mol%K^+. (f) Integrated emission intensity as a function of temperature of Ba_2GdGaO_5:3 mol%Bi^{3+} and Ba_2GdGaO_5:3 mol%Bi^{3+}, 2 mol%K^+.

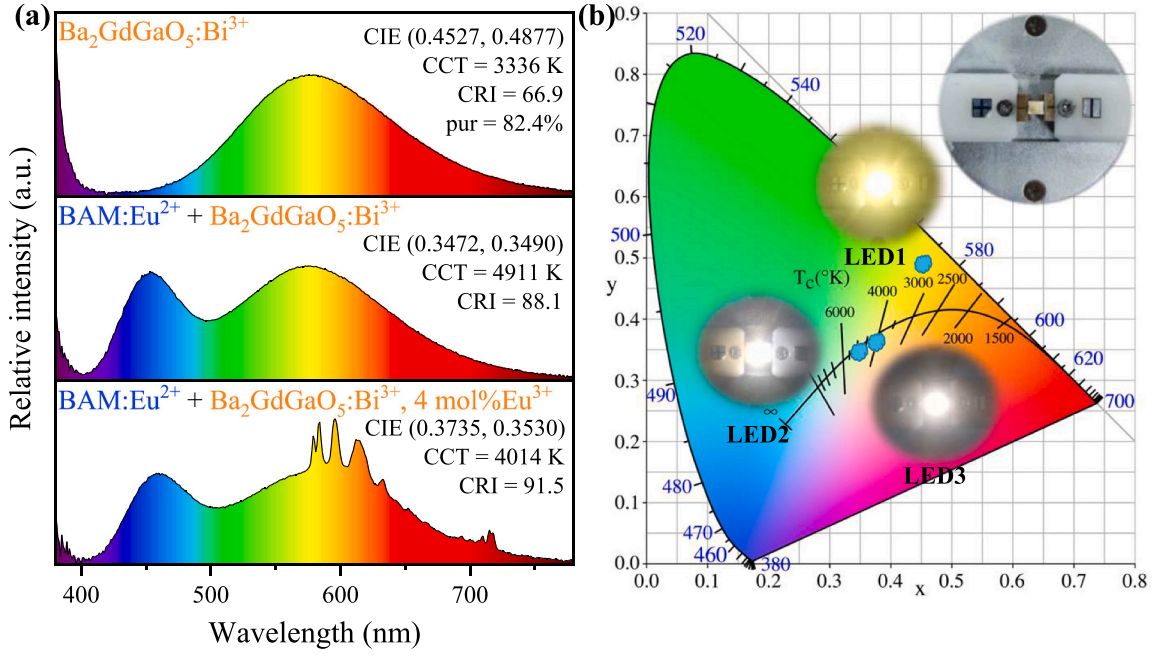

Fig. 8. (a) EL spectra of as-fabricated pc-LED. (b) CIE chromaticity coordinates and pc-LED photographs.

relationship between crystal structure and luminescent mechanism is studied in detail. K^+ doping as flux can improve the crystallinity of the material, and thus enhance the PL intensity of Ba_2GdGaO_5:3 mol%Bi^{3+} phosphor to 133.1% excited at 365 nm. Finally, through the preparation of pc-WLED, the application potential in the field of warm white light is demonstrated. A pc-WLED is prepared by combining Ba_2GdGaO_5:3 mol %Bi^{3+} with BAM:Eu^{2+} phosphor, which shows a CRI of 88.1 and a CCT of 4911 K. The CRI is increased to 91.5 and the CCT is lowered to 4014 K by doping with Eu^{3+}, and the warm white light emission is obtained.

Author contributions

Ke Chen and Peixin Gao contributed equally to this work. The manuscript was written through contributions of all authors. All authors have given approval to the final version of the manuscript.

CRediT authorship contribution statement

Peixin Gao: Writing – review & editing, Writing – original draft. **Zengtao Zhang:** Writing – review & editing. **Yibiao Ma:** Writing – review & editing. **Zan Luo:** Writing – review & editing. **Ke Chen:** Writing – review & editing, Writing – original draft. **Zhi Zhou:** Supervision, Resources. **Maxim S Molokeev:** Methodology, Data curation. **Mao Xia:** Supervision, Resources.

Declaration of Competing Interest

The authors declare that they have no known competing financial interests or personal relationships that could have appeared to influence the work reported in this paper.

Data Availability

Data will be made available on request.

Acknowledgements

The authors would like to gratefully acknowledge funds from the National Natural Science Foundation of China (Grant No. 51974123), the Key R & D Projects in Hunan Province (2021SK2047 and 2022NK2044), the Wangcheng Science and Technology Plan (KJ221017) and the Science and Technology Innovation Program of Hunan Province (2022WZ1022). The work was supported by the Ministry of Science and Higher Education of the Russian Federation as part of World-class Research Center program: ‘‘Advanced Digital Technologies’’, contract no. 075-15-2020-935. Superior Youth Project of the Science Research Project of Hunan Provincial Department of Education (22B0211).

References

[1] M.H. Fang, Z. Bao, W.T. Huang, R.S. Liu, Evolutionary generation of phosphor materials and their progress in future applications for light-emitting diodes, Chem. Rev. 112 (2022) 11474–11513.
[2] P.P. Dang, G.G. Li, X.H. Yun, Q.Q. Zhang, D.J. Liu, H.Z. Lian, M.M. Shang, J. Lin Thermally stable and highly efficient red-emitting Eu^{3+}-doped $Cs_3GdGe_3O_9$ phosphors for WLEDs: non-concentration quenching and negative thermal expansion, Light Sci. Appl. 10 (2021) 29.
[3] M.D. Mehare, C.M. Mehare, H.C. Swart, S.J. Dhoble, Recent development in color tunable phosphors: a review, Prog. Mater. Sci. 133 (2023) 101067–101118.
[4] G.B. Nair, H.C. Swart, S.J. Dhoble, A review on the advancements in phosphor-converted light emitting diodes (pc-LEDs): phosphor synthesis, device fabrication and characterization, Prog. Mater. Sci. 109 (2020) 100622–100658.
[5] S. Zhang, Y. Liu, J. Yin, X. Zhang, Y. Li, L. Su, Z. Zhou, M. Xia, A novel Cr^{3+}-activated far-red titanate phosphor: synthesis, luminescence enhancement and application prospect, Mater. Today Chem. 24 (2022) 100835.
[6] Q. Yao, P. Hu, P. Sun, M. Liu, R. Dong, K.F. Chao, Y.F. Liu, J. Jiang, H.C. Jiang, YAG:Ce^{3+} Transparent ceramic phosphors brighten the next-generation laser-driven lighting, Adv. Mater. 32 (2020) 1907888–1907894.
[7] M. Zhao, Z.Y. Yang, L.X. Ning, Z.G. Xia Tailoring, of White Luminescence in a $NaLi_3SiO_4$:Eu^{2+} Phosphor Containing Broad-Band Defect-Induced Charge-Transfer Emission, Adv. Mater. 33 (2021) 2101428.
[8] L.J. Wu, P.P. Dai, D. W, Wen new structural design strategy: optical center VO_4-activated broadband yellow phosphate phosphors for high-color-rendering WLEDs, ACS Sustain. Chem. Eng. 10 (2022) 3757–3765.
[9] S.Q. Lai, M. Zhao, Y.F. Zhao, M.S. Molokeev, Z.G. Xia, Eu^{2+} Doping concentration-induced site-selective occupation and photoluminescence tuning in $KSrScSi_2O_7$:Eu^{2+} Phosphor, ACS Mater. Au. 2 (2022) 374–380.
[10] P.X. Gao, Q. Li, C. Zhou, K. Chen, Z. Luo, S.J. Zhang, M.S. Molokeev, J. Wang, Z. Zhou, M. Xia, High-efficiency continuous-luminescence-controllable performance and antithermal quenching in Bi^{3+}-activated phosphors, Inorg. Chem. 61 (2022) 13104–13114.
[11] Z.H. Leng, H. Bai, Q. Qing, H.B. He, J.Y. Hou, B.Y. Li, Z.B. Tang, F. Song, H.Y. Wu, A Zero-Thermal-Quenching Blue Phosphor for Sustainable and Human-Centric WLED Lighting, ACS Sustain. Chem. Eng. 10 (2022) 10966–10977.
[12] R. Shi, X.J. Zhang, Z.X. Qiu, J.L. Zhang, S.Z. Liao, W.L. Zhou, X.H. Xu, L.P. Yu, S. X. Lian, Composition and antithermal quenching of noninteger stoichiometric Eu^{2+}-Doped na-beta-alumina with cyan emission for near-UV WLEDs, Inorg. Chem. 60 (2021) 19393–19401.
[13] W. Yan, S.T. Chen, Y.X. Liu, Z.Y. Gao, Y. Wei, G.G. Li, Giant photoluminescence Improvement and Controllable Emission Adjustment in Bi^{3+}-Activated $Ca_4ZrGe_3O_{12}$ Phosphors for high-quality white light-emitting diodes, ACS Appl. Electron. Ma. 1 (2019) 1970–1980.
[14] Y.B. Fu, P.X. Xiong, X.Q. Liu, X. Wang, S. Wu, Q. Liu, M.Y. Peng, Y. Chen, A promising blue-emitting phosphor $CaYGaO_4$:Bi^{3+} for near-ultraviolet (NUV) pumped white LED application and the emission improvement by Li^+ ions, J. Mater. Chem. C. 9 (2021) 303–312.
[15] Z.G. Xia, A. Meijerink $Ce3^+$-Doped garnet phosphors: composition modification, luminescence properties and applications, Chem. Soc. Rev. 46 (2017) 275–299.
[16] G.G. Li, Y. Tian, Y. Zhao, J. Lin, Recent progress in luminescence tuning of Ce^{3+} and Eu^{2+}-activated phosphors for pc-WLEDs, Chem. Soc. Rev. 44 (2015) 8688–8713.
[17] S.W. Wang, H.Y. Wu, Y.F. Fan, Q. Wang, T. Tan, R. Pang, S. Zhang, D. Li, L. H. Jiang, C.Y. Li, et al., A highly efficient narrow-band blue phosphor of Bi^{3+}-activated cubic borate $Ba_3Lu_2B_6O_{15}$ towards backlight display applications, Chem. Eng. J. 432 (2022) 134265–134272.
[18] Q.S. Wu, Y.Y. Li, Y.J. Wang, H. Liu, S.S. Ye, L. Zhao, J.Y. Ding, J.C. Zhou, A novel narrow-band blue-emitting phosphor of Bi^{3+}-activated $Sr_3Lu_2Ge_3O_{12}$ based on a highly symmetrical crystal structure used for WLEDs and FEDs, Chem. Eng. J. 401 (2020) 126130–126140.
[19] M.S. Cai, T.C. Lang, T. Han, D. Valiev, S.Q. Fang, C.Z. Guo, S.S. He, L.L. Peng, S. X. Cao, B.T. Liu, et al., Novel Cyan-Green-Emitting Bi^{3+}-Doped $BaScO_2F$, R^+ (R = Na, K, Rb) Perovskite Used for Achieving Full-Visible-Spectrum LED Lighting, Inorg. Chem. 60 (2021) 15519–15528.
[20] Z. Zhou, N. Zhou, M. Xia, M. Yokoyama, H.T. Hintzen, Research progress and application prospects of transition metal Mn^{4+}-activated luminescent materials, J. Mater. Chem. C. 4 (2016) 9143–9161.
[21] S.S. Liang, D.C. Huang, J. Hu, D.J. Chen, K.Y. Xu, H.M. Zhu, A highly efficient red emitting phosphor with enhanced blue-light absorption through a local crystal field regulation strategy, Chem. Eng. J. 429 (2022) 132003.
[22] S.M. Gu, M. Xia, C. Zhou, Z.H. Kong, M.S. Molokeev, L. Liu, W.Y. Wong, Z. Zhou, Red shift properties, crystal field theory and nephelauxetic effect on Mn^{4+}-doped $SrMgAl_{10-y}Ga_yO_{17}$ red phosphor for plant growth LED light, Chem. Eng. J. 396 (2020) 125208.
[23] P.P. Dang, D.J. Liu, G.G. Li, A.A. Al Kheraif, J. Lin, Recent Advances in Bismuth Ion-Doped Phosphor Materials: Structure Design, Tunable Photoluminescence Properties, and Application in White LEDs, Adv. Opt. Mater. 8 (2020) 1901993–1902052.
[24] F. Du, Z.B. Tang, Q.Q. Zhao, L.S. Du, W.Q. Xia, $Ba_5GeO_4Br_6$:Bi^{3+}, a promising cyan phosphor for high-quality full-spectrum white light illumination, J. Lumin. 255 (2023) 119592–119599.
[25] Z.C. Liao, L.T. Qiu, X.T. Wei, Y.H. Chen, Study on luminescence properties of Bi^{3+} doped Ba_2YAlO_5: A wide-band yellow emitting phosphor with excellent thermal stability, J. Alloy Compd. 938 (2023) 168648–168657.
[26] H.M. Li, R. Pang, Y.Q. Luo, H.Y. Wu, S. Zhang, L.H. Jiang, D. Li, C.Y. Li, H.J. Zhang, Structural Micromodulation on Bi^{3+}-Doped $Ba_2Ga_2GeO_7$ Phosphor with Considerable Tunability of the Defect-Oriented Optical Properties, ACS Appl. Electron. Ma. 1 (2019) 229–237.
[27] F.W. Kang, H.S. Zhang, L. Wondraczek, X.B. Yang, Y. Zhang, D.Y. Lei, M.Y. Peng, Band-Gap Modulation in Single Bi^{3+}-Doped Yttrium–Scandium–Niobium Vanadates for Color Tuning over the Whole Visible Spectrum, Chem. Mater. 28 (2016) 2692–2703.
[28] Y. Wei, H. Yang, Z.Y. Gao, G.C. Xing, M.S. Molokeev, G.G. Li, Bismuth activated full spectral double perovskite luminescence materials by excitation and valence control for future intelligent LED lighting, Chem. Commun. 56 (2020) 9170–9173.
[29] P.P. Dang, D.J. Liu, X.H. Yun, G.G. Li, D.Y. Huang, H.Z. Lian, M.M. Shang, J. Lin, Ultra-broadband cyan-to-orange emitting $Ba_{1+x}Sr_{1-x}Ga_4O_8$:Bi^{3+} phosphors: luminescence control and optical temperature sensing, J. Mater. Chem. C. 8 (2020) 1598–1607.
[30] X.Y. Zhu, T. Wang, H.Z. Liu, L. Nie, F. Zhao, S.F. Yu, J.B. Qiu, X.H. Xu, X. Yu, Achievement of full-visible-spectrum lighting in Bi^{3+}-activated strontium gallates via lattice site occupancy engineering toward WLEDs applications, Mater. Today Phys. 31 (2023) 100968.

[31] W. Yan, Y. Wei, M.S. Molokeev, S. Wang, G.G. Li, Green-emitting $Bi3^{+}$-doped $La_2SrSc_2O_7$ phosphor for pc-WLED lighting: Luminescent properties and energy transfer strategy, J. Alloy Compd. 908 (2022) 164621–164632.
[32] L. Liu, S.S. Peng, L. Fu, Y.X. Guo, X. Sun, L. Song, J.P. Shi, Y. Zhang, Closing the Deep-Blue Gap: Realizing Narrow-Band Deep-Blue Emission with Strong n-UV Excitation by Cationic Substitution for Full-Spectrum Warm W-LED Lighting, ACS Sustain. Chem. Eng. 10 (2022) 6190–6195.
[33] S.J. Gai, P.X. Gao, K. Chen, C.Z. Tang, Y.Y. Zhao, J.Q. Wei, Y. Zhang, M. S. Molokeev, M. Xia, Z. Zhou, Superior Quantum Efficiency Blue-Emitting Phosphors with High Thermal Stability toward Multipurpose LED Applications, Adv. Opt. Mater. 2302880 (2024) 2302870.
[34] P.X. Gao, Q. Li, S.Y. Li, S.J. Gai, Y.N. Li, Y.B. Ma, Z.T. Zhang, M.S. Molokeev, Z. Zhou, M. Xia, Multiple Strategies to Approach High-Efficiency Luminescence Controllable in Blue/Cyan/Green-Emitting Bi^{3+}-Activated Phosphors, J. Phys. Chem. C. 126 (2022) 9195–9206.
[35] D.J. Liu, P.P. Dang, X.H. Yun, G.G. Li, H.Z. Lian, J. Lin, Luminescence color tuning and energy transfer properties in $(Sr,Ba)_2LaGaO_5:Bi^{3+},Eu^{3+}$ solid solution phosphors: realization of single-phased white emission for WLEDs, J. Mater. Chem. C. 7 (2019) 13536–13547.
[36] D.J. Liu, X.H. Yun, P.P. Dang, H.Z. Lian, M.M. Shang, G.G. Li, J. Lin, Yellow/Orange-Emitting $ABZn_2Ga_2O_7:Bi^{3+}$ (A = Ca, Sr; B = Ba, Sr) Phosphors: Optical Temperature Sensing and White Light-Emitting Diode Applications, Chem. Mater. 32 (2020) 3065–3077.
[37] S. Wu, Q. Liu, P.X. Xiong, W.W. Chen, Q. Dong, D.D. Chen, D. Wang, G.X. Zhang, Y. Chen, G.G. Li, Single Bi^{3+} Ultrabroadband White Luminescence in Double Perovskite via Crystal Lattice Engineering toward Light-Emitting Diode Applications, Adv. Opt. Mater. 10 (2022) 2102842–2102852.
[38] H.M. Li, R. Pang, G.Y. Liu, W.Z. Sun, D. Li, L.H. Jiang, S. Zhang, C.Y. Li, J. Feng, H. J. Zhang Synthesis and Luminescence Properties of Bi^{3+}-Activated K_2MgGeO_4: A Promising High-Brightness Orange-Emitting Phosphor for WLEDs Conversion, Inorg. Chem. 57 (2018) 12303–12311.
[39] P.P. Dang, Q.Q. Zhang, D.J. Liu, G.G. Li, H.Z. Lian, M.M. Shang, J. Lin, Heterovalent substitution strategy toward orange-red luminescence in Bi^{3+} doped layered perovskite oxide phosphors for high color rendering index white light-emitting diodes, Chem. Eng. J. 420 (2021) 127640–127649.
[40] H.Z. Zhang, J. Zhang, Y.C. Su, X.M. Zhang Metal, To Metal Charge Transfer Induced Efficient Yellow/Far-Red Luminescence in $Na_2Ca_3(Nb, Ta)_2O_9:Bi^{3+}$ toward the Applications of White-LEDs and Plant Growth Light, Adv. Opt. Mater. 10 (2022) 2200150–2200159.
[41] X.J. Zhang, Y.B. Ma, P.X. Gao, L.J. Su, Z.T. Zhang, Z. Zhou, X.Y. Lu, M. Xia, Accessing deep-red emission using chemical units cosubstituted $LaTiSbO_6:Mn^{4+}$ phosphor, Ceram. Int. 48 (2022) 29547–29553.
[42] Y.S. Lian, Y. Wang, J.F. Li, Z.J. Zhu, Z.Y. You, C.Y. Tu, Y.D. Xu, W.Q. Jie, Structural and optical properties of $Dy^{3+}:YAlO_3$ phosphors for yellow light-emitting diode applications, J. Rare Earth 39 (2021) 889–896.
[43] Q. Wang, Z.J. Liang, J.C. Luo, Y. Yang, Z.F. Mu, X. Zhang, H.F. Dong, F.G. Fu, Ratiometric optical thermometer with high sensitivity based on dual far-red emission of Cr^{3+} in $Sr_2MgAl_{22}O_{36}$, Ceram. Int. 46 (2020) 5008–5014.
[44] L.G. Van Uitert, Characterization of Energy Transfer Interactions between Rare Earth Ions, J. Electrochem Soc. 114 (1967) 1048–1053.
[45] T.Q. Zhang, X.L. Jiang, R. j Chen, B.Y. Liu, W.L. Yang, C. Li, H. Lin, H.S. Liu, C. Li, F.M. Zeng, et al., A blue-emitting Eu^{2+}-activated $BaZnAl_{10}O_{17}$ phosphor for white light emitting diodes: structure and luminescence properties, Inorg. Chem. Front. 9 (2022) 6418–6424.
[46] Y. Zhong, Y. Zhou, C. Zhou, H.X. Chen, Z. Zhou, M.G. Brik, M. Xia, Two targets with one strategy: Insights into the role of aluminum atoms on the luminescence properties and thermal stability in Mn^{4+}-doped calcium aluminozincate phosphor, J. Alloy Compd. 849 (2020) 156567.
[47] J.W. Qiao, G.J. Zhou, Y.Y. Zhou, Q.Y. Zhang, Z.G. Xia, Divalent europium-doped near-infrared-emitting phosphor for light-emitting diodes, Nat. Commun. 10 (2019) 5267.
[48] P.X. Gao, Q. Li, C. Zhou, K. Chen, Z. Luo, S.J. Zhang, M.S. Molokeev, J. Wang, Z. Zhou, M. Xia, High-efficiency continuous-luminescence-controllable performance and antithermal quenching in bi3+-activated phosphors, Inorg. Chem. 61 (2022) 13104–13114.
[49] H.F. Yang, P.L. Li, Z.J. Ye, X.X. Huo, Y. Wang, Q. Wu, Z.J. Wang, Improving the luminescence property of the novel yellow-emitting phosphor $SrLa_2Sc_2O_7:Bi^{3+}$ with charge compensators (Li^{+}, Na^{+}, K^{+}) and its application in NUV-based white LEDs, Dalton Trans. 51 (2022) 16628–16638.
[50] M. Xia, Y.L. Zhang, M.H. Li, Y. Zhong, S.M. Gu, N. Zhou, Z. Zhou High, thermal stability and blue-violet emitting phosphor $CaYAlO_4:Ti^{4+}$ with enhanced emission by Ca^{2+} vacancies, J. Rare Earth 38 (2020) 227–233.
[51] J.W. Qiao, S. Zhang, X.Q. Zhou, W.B. Chen, R. Gautier, Z.G. Xia, Near-Infrared Light-Emitting Diodes utilizing a Europium-Activated Calcium Oxide Phosphor with External Quantum Efficiency of up to 54.7%, Adv. Mater. 34 (2022) 2201887.
[52] S.S. Ye, J.Y. Ding, Q.S. Wu, MMCT-induced high-bright yellow light-emitting phosphor Bi^{3+}-activated Ba_2YGaO_5 used for WLED, Chem. Eng. J. 428 (2022) 131238.